Journal of Nuclear Materials 406 (2010) 39–54

Contents lists available at ScienceDirect

Journal of Nuclear Materials

journal homepage: www.elsevier.com/locate/jnucmat

Modeling the long-term evolution of the primary damage in ferritic alloys using coarse-grained methods

C.S. Becquart [a,*], A. Barbu [b], J.L. Bocquet [b], M.J. Caturla [c], C. Domain [d], C.-C. Fu [b], S.I. Golubov [e,j], M. Hou [f], L. Malerba [g], C.J. Ortiz [c,h], A. Souidi [i], R.E. Stoller [j]

[a] Unité Matériaux et Techniques (UMET), UMR 8207, Université Lille-1, F-59655 Villeneuve d'Ascq Cédex, France
[b] Service de Recherches de Métallurgie Physique, CEA Saclay, F-91191 Gif-sur-Yvette, France
[c] Dept. Física Aplicada, Universidad de Alicante, Alicante E-03690, Spain
[d] EDF-R&D Département MMC, Les Renardières, F-77818 Moret sur Loing Cédex, France
[e] Center for Materials Processing, University of Tennessee, East Stadium Hall, Knoxville, TN 37996-0750, USA
[f] Physique des Solides Irradiés et des Nanostructures CP234, Université Libre de Bruxelles, Bd du Triomphe, B-1050 Brussels, Belgium
[g] Structural Materials Group, Nuclear Materials Science Institute, SCK–CEN, Boeretang 200, B-2400 Mol, Belgium
[h] Laboratorio de Fusión por Confinamiento Magnético, CIEMAT, E-28040 Madrid, Spain
[i] Centre Universitaire de Saida, BP138 En Nasr, Saida 20000, Algeria
[j] Materials Science and Technology Division, Oak Ridge National Laboratory, P.O. Box 2008, Oak Ridge, TN 37831-6138, USA

A B S T R A C T

Knowledge of the long-term evolution of the microstructure after introduction of primary damage is an essential ingredient in understanding mechanical property changes that occur during irradiation. Within the European integrated project "PERFECT," different techniques have been developed or improved to model microstructure evolution of Fe alloys under irradiation. This review paper aims to present the current state of the art of these techniques, as developed in the project, as well as the main results obtained.

1. Introduction

One of the objectives of the European 6th Framework Programme Integrated Project PERFECT (henceforth, the Project) was the development of models describing the long-term evolution induced by primary radiation damage in Fe alloys. Models based on the chemical reaction rate theory (alternatively transition state theory) are commonly applied for this purpose. These models typically employ either the kinetic Monte-Carlo (KMC) or the mean field (effective medium) method. The mean field models have been used so widely for so long that the use of the name "rate theory" is commonly thought to imply a mean field model. To be clear, the term mean field rate theory (MFRT) is used here. Both KMC and MFRT can be globally defined as coarse-grained models because atoms are not explicitly treated in either. Note however, that this does not hold true in the case of lattice (or atomistic) KMC, which is described in more details in [1]. The species under consideration are defects whose atomic-level features are disregarded, except insofar as they influence the mechanisms whereby the defects migrate or react between themselves and with sinks. It is important to stress out that KMC and MFRT methods are methods intended to simulate the time evolution of some processes occurring in nature. Typically these are processes that occur with a given known rate, which are inputs to the algorithms. These methods do not have the capability to predict structures or events that are not explicitly included in the model (unlike *ab initio* or MD simulations). Although the two methods, KMC and MFRT, require the same physical and material input parameters, and provide the same type of output, their implementations of the rate theory differ in many aspects. A primary difference between the two methods is that spatial information about individual objects is maintained in KMC, while only spatially averaged information is used in the MFRT. Furthermore, KMC (in both versions discussed here, namely Object and Event KMC, see below) deal with the explicit spatial dependence of the evolving defect distribution. In contrast, MFRT models do not deal with the explicit position of defects but deal with the averaged concentration of defects in a small volume at a given position in the material. However, it must be emphasized that MFRT models do take into account the presence of gradients of concentration and hence, in some sense, deal with the spatial dependence of the evolving defect distribution.

The present paper reviews the work performed within the project on these type of models, with an emphasis on the KMC method and a comparison between KMC and MFRT. The work on atomistic KMC (AKMC) models is reviewed in [1], while a discussion of the

* Corresponding author. Tel.: +33 320 436927; fax: +33 320 434040.
E-mail address: charlotte.becquart@univ-lillel.fr (C.S. Becquart).

0022-3115/$ - see front matter © 2010 Elsevier B.V. All rights reserved.
doi:10.1016/j.jnucmat.2010.05.019

main differences between KMC and MFRT, including their advantages and drawbacks, is provided in [2–4].

In general terms, the KMC method provides a solution to the Master Equation which describes a physical system whose evolution is governed by a known set of transition rates between possible states. The solution proceeds by choosing randomly among the various possible transitions and accepting them on the basis of probabilities that depend directly on the corresponding transition rates [5]. When applied to study the evolution of systems of mobile species, such as atoms [6–8] or defects formed under irradiation [9–11] it has the advantage of going beyond the mean-field approximation [12], by explicitly accounting for spatial correlations between the elements of the physical system and the overall geometry of the system.

A variety of coarse-grained KMC models have been formulated to describe the long-term evolution of the primary damage produced by irradiation. In some models, defect migration jumps are explicitly treated and reactions occur when two defects (mobile objects) meet each other, or meet traps and/or sinks. Other models do not treat individual migration jumps explicitly and only reactions (events) between objects drive the evolution of the system. The former type of model is denoted here as Object KMC (OKMC), the latter as Event KMC (EKMC). Both approaches have been pursued within the project and, whenever possible, comparison exercises have been performed.

2. General features of the KMC methods and codes

Different methods and codes have been used in the framework of the Project, two implementing an OKMC approach (LAKIMOCA, BIGMAC) and one implementing an EKMC approach (JERK). Even when the approach is the same, some differences in the implementation exist. In the following section, the general OKMC algorithm is summarized. The specifics of each OKMC code are then separately addressed. Finally, the EKMC algorithm and its implementation in JERK are described.

2.1. The OKMC algorithm

The OKMC method is based on the residence time algorithm (RTA), also known as the BKL method (for Bortz, Kalos and Lebowitz) [13]. This algorithm is used to evolve a set of objects that can undergo different events. Given a set of possible events involving these objects, $\{e_i;\ i = 1, \ldots, N_e\}$, each with a known rate of occurrence, Γ_i, a total rate, R, is computed as the sum over all N_e events of the product $\Gamma_i n_i$, where n_i is the number of events of the same type with the same rate:

$$R = \sum_{i=1}^{N_e} n_i \Gamma_i \tag{1}$$

A Monte-Carlo step is initiated by selecting an event from all N_e based on a random number between 0 and R. The value of this number determines which event is selected since the increment due to each event in the interval [0:R] in Eq. (1) is known. If more than one object can undergo the selected event, one is chosen at random. Once the event and the corresponding object are selected, the appropriate actions are performed to make that event occur and the time is updated, by adding a time increment proportional to the inverse of R:

$$\delta\tau = \frac{-\log \xi}{R} \tag{2}$$

where ξ is a random number in the interval [0, 1], which is included to ensure a Poisson distribution of the time increments. In the limit of long times, it is easy to demonstrate that the average, $\delta\tau \to 1/R$, which is the average time increment. Thus, this average value can also be used in the KMC algorithm as initially proposed by [14].

This general algorithm can be applied to study a wide variety of processes. In the case of the long-term evolution of radiation damage the objects are the intrinsic defects (vacancies and self-interstitials) or impurities, and their clusters which are located at known (and traced) positions in a simulation volume. The events are all the possible actions that these objects can perform and the reactions that they may undergo, such as: (a) migration, (b) dissociation (emission of a smaller defect from a bigger one), (c) aggregation of like defects or of defects and impurities, and (d) annihilation between opposite defects (self-interstitials and vacancies). A pictorial representation of these events in given in Fig. 1.

The probability for a migration event is given by the corresponding jump frequency, expressed as a thermally activated process, following the Arrhenius dependence:

$$\Gamma_m = \Gamma_0 \exp\left(\frac{-E_m}{k_B T}\right) \tag{3}$$

where Γ_0 is the attempt frequency, which can be taken as a constant prefactor, on the order of the Debye frequency; E_m is the migration energy of that particular object; T is the temperature; and k_B the Boltzmann constant.

For the dissociation events, the probability is given in terms of a jump frequency, with an activation energy equal to the sum of the migration energy plus the binding energy between the emitted defect and a cluster of the size that remains after emission, E_b:

$$\Gamma_d = \Gamma_0 \exp\left(-\frac{E_m + E_b}{k_B T}\right) \tag{4}$$

E_b will in general depend on the type of emitted and emitting object, as well as on the emitting object's size.

For the case of events of type (c) and (d), which are reactions between defects, it is generally assumed that they are *diffusion-limited*. That is, the reaction occurs as soon as the two objects are within a pre-defined capture radius, but no energy barrier is associated with the reaction. These events occur therefore only on the basis of geometrical considerations (overlap of reaction volumes) and do not participate in defining the progressing of time. Events of this type also include the absorption of objects by sinks (dislocations, grain boundaries, ...).

However, other events due to external processes which involve objects that are not contained in the simulation volume need to be included in radiation damage simulation and these do influence the rate at which time progresses. These are events producing damage, such as the appearance of isolated Frenkel pairs (FP), as in electron irradiation, or of the debris of a displacement cascade, as in ion or neutron irradiation. Since each of these N_e^{ext} possible external events occurs at a known rate, P_j, these rates must be included in the computation of the total rate, R, and the corresponding generalization of Eq. (2), in the limit of long times (i.e. without the logarithm of the random number), becomes

$$\delta\tau = 1 \Big/ \left(\sum_{i=1}^{N_e} \Gamma_i + \sum_{j=1}^{N_e^{ext}} P_j\right) \tag{5}$$

Difficulties in applying the OKMC algorithm are not due to the method itself, which is fairly straightforward. These stem, instead, from the fact that all the possible events that each object can undergo according to a specific physical mechanism, their appropriate probability, and their defining properties must be predefined. These will change from object to object. For example, let us take a single vacancy, V, a di-vacancy, V_2, and a single self-interstitial I. The forward reactions that these objects can undergo (e.g. the annihilation of the vacancy with the self-interstitial: $V + I \to 0$; or formation of a tri-vacancy: $V + V_2 \to V_3$) will occur depending on

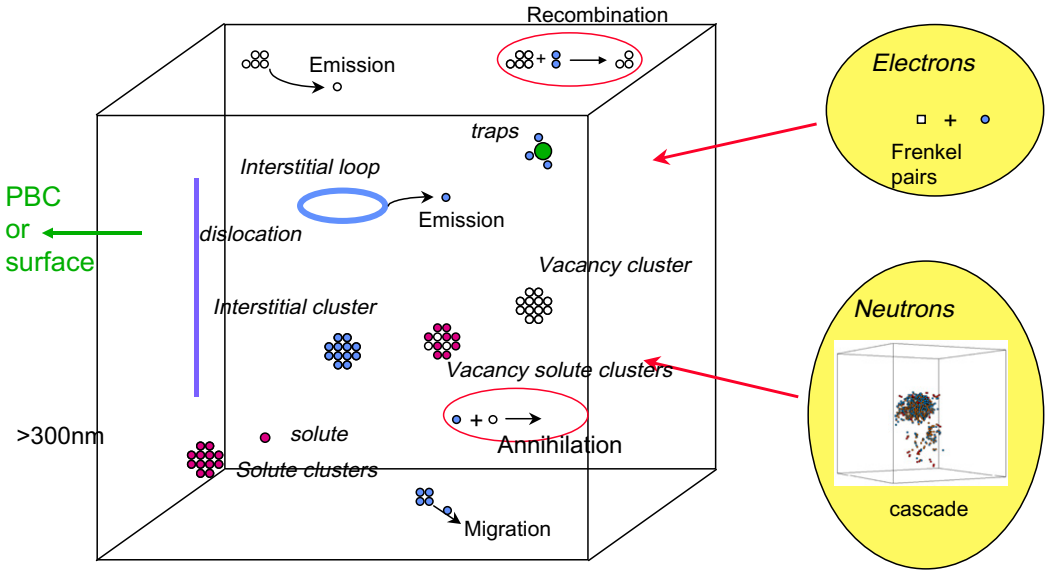

Fig. 1. Summary of the different possible events taking place in an object KMC simulation (LAKIMOCA).

the respective capture radii. The capture radius will be different depending on the defect size (it will grow going from V to V_3). The backward reactions (e.g. the dissociation of a vacancy from a di-vacancy: $V_2 \rightarrow V + V$; or from a tri-vacancy: $V_3 \rightarrow V_2 + V$) will depend on the migration energy of the single vacancy and the binding energy of the latter to the di- (or tri-) vacancy. The binding energy will be different depending on the emitting defect (V_2 or V_3). Finally, the probability of migration of each object will depend on its migration energy and, again, V and V_2 must be considered *a priori* as different objects for migration purposes. In addition, the migration mechanism can vary; for example, clusters of self-interstitials may migrate in one-dimension only. Therefore vacancy and self-interstitial cluster properties must be pre-defined up to a size that is considered large enough for the specifically studied problem. The problem of pre-defining possible actions, reactions, mechanisms and parameters for all possible objects is here denoted as the "code parameterisation" problem, and is addressed in Section 3.

2.1.1. The OKMC code LAKIMOCA

The LAKIMOCA code has been developed at EDF, and has been extensively described in a previous publication [11]. The code allows easy introduction of different classes of immobile traps and sinks, characterized by specific geometrical shapes (spheres, infinite cylinders, surfaces, etc.) and suitable for mimicking voids or other trapping nano-features, as well as dislocations and grain boundaries [15]. The code is therefore equipped to mimic fairly realistic microstructures and irradiation conditions.

The objects (or more precisely their center of mass) are located on a lattice, which is simply the atomic lattice and changes depending on the materials modeled. The jump of a mobile object is from one lattice site to a first neighbor lattice site; the coordinates of the objects are thus integer (i, j, k) coordinates and the dimensionality of the motion according to specific crystallographic directions is easily controlled. New radiation-induced defects can be either randomly introduced as FP in the simulation box or read from a file (e.g. the cascade debris obtained by molecular dynamics, MD). The vacancy and the interstitial from a FP can be spatially correlated using a separation criterion. To model ion implantation, the individual defects or cascades can be introduced using a specific distribution profile along a direction. Dislocation loops can be modeled as having either a spherical or disk-like shape.

The defect properties (where by defects we mean vacancies and self-interstitials, but also foreign atoms, e.g. copper or helium atoms) are defined in specific files containing the mobility of the defects (i.e. the prefactor and the migration energy), their binding energies for emission, and their reaction radii. The diffusion of the defects is 3D by default, but a 1D diffusion with thermally activated direction changes is also implemented. Traps and sinks are characterized by their recombination radii and binding energies. In principle, in an OKMC model it is possible to take into account long range interactions, due to misfit strain, by having the binding and migration energies depend on each other's strain field, via elastic interaction rules. This feature, however, is currently not implemented in the LAKIMOCA code.

2.1.2. The OKMC code BIGMAC

The kinetic Monte-Carlo code BIGMAC was developed at Lawrence Livermore National Laboratory by M. Johnson in collaboration with M.J. Caturla and T. Díaz de la Rubia [16]. This code has been used by different research groups to study many different systems, including Si [17], Cu [9], Pb [18], Fe [10,19], V [20] and Zr [21].

In the most general form of the code there is not an underlying lattice, therefore defects are located at random positions. However, it is possible to modify the code to include a lattice if necessary [22]. The position of the defects are defined by their (x, y, z) coordinates. The initial defect distribution can be defined by two different methods. A concentration profile can be given as a function of depth such that defects are created randomly in the simulation box to provide the right profile. Alternatively, the (x, y, z) coordinates of each defect can be read from a file, as could be in the case of defect positions calculated from other simulation tools such as MD or binary collision approximation (BCA) methods [23].

One of the particular features of BIGMAC is its versatility for creating new objects and new events. The user defines each of the objects that he wants to include in the simulation and all of the possible events that object can perform, with their appropriate probabilities and capture radii, in a set of input files. For instance, there is an input file that defines the interaction of each object with each one of the surfaces of the simulation box. A value between 0 and 1 can be given to each object where 0 means a total reflecting surface and 1 is a total absorbing surface. The fact that there are no hardwired reactions in the code allows the user to define any type of system that he/she is interested in studying, having to define

each object and each reaction. This versatility allowed the study of complex systems such as Fe–He–C, including intrinsic defects (vacancies and self-interstitials), He–vacancy complexes, C–vacancy complexes, as well as He–C–vacancy complexes. The disadvantage of this approach appears for very high doses, where large defect clusters are formed, since it requires large memory to store the matrices for all defect reactions. A preliminary version of the code, not yet released, allows for the growth and dissociation of clusters internally in the code, therefore only the species are defined (vacancies, self-interstitials, He–V, etc.) without having to define each size independently.

As mentioned earlier, the general version of the code does not have an underlying lattice. Therefore, when an object is selected to migrate it is displaced a fixed distance, the jump distance, λ, normally taken as the nearest neighbor distance for the system of interest. The objects can be defined to migrate in three dimensions or in one-dimension. If the migration is three-dimensional, the new position of the particle will be selected randomly at the edge of a sphere of radius the jump distance λ. For one dimensional migration, the object will be displaced the jump distance in the direction of interest. It is important to point out that the code is flexible enough to allow for the reaction of two objects to form as many resulting objects as selected by the user, and a single object can perform as many backward reactions (dissociation reactions) as defined by the user. This is important when complex clusters are included as can be the case of He–C–V where any of the three components could be the dissociating object.

2.2. The EKMC algorithm and the code JERK

The general features of the JERK code were originally given in [24] and have been recalled in more detail in [25]. The crystal lattice is ignored and objects' coordinates can change continuously. The only events considered are those which lead to a change in the defect population, namely: clustering of objects, emission of mobile species, elimination of objects on fixed sinks (surface, dislocation), or the annihilation of objects on their anti-defect. The migration of an object in its own right is considered an event only if it ends up with a reaction which changes the defect population. In this case the migration step and the reaction are processed as a single event; otherwise, the migration is performed only once at the end of the EKMC time interval Δt. The role and the choice of Δt are discussed below.

In contrast to the residence time algorithm, where all rates are lumped into one total rate to obtain the time increment (Eqs. (2) and (5)), in an EKMC scheme the time delays of all possible events are calculated separately and sorted by increasing order in a list. The event corresponding to the shortest delay, τ_s, is processed first, and the remaining list of delay times for other events is modified accordingly by eliminating the delay time associated with the particle that just disappeared, adding delay times for a new mobile object, etc. The actual time is increased by τ_s and the next event on the list is processed until all possible events that can happen before time Δt have occurred. The delay times that include a migration step are calculated according to continuous laws of diffusion, after converting jump frequencies Γ_i into diffusion coefficients D_i. For a walker starting at a distance d from a partner of radius r, the probability that they will meet is given by:

$$P(d,t) = \frac{r}{d} erfc\left\{\frac{d-r}{2\sqrt{Dt}}\right\} \tag{6}$$

which is easily inverted to yield the time delay under the form:

$$\tau = \frac{1}{4D}\frac{(d-r)^2}{\{erfc^{-1}(\xi d/r)\}^2} \tag{7}$$

where $erfc^{-1}$ is the inverse of the complementary error function and ξ is a random number uniformly distributed over [0, 1]. This delay is calculated in the framework of a binary collision approximation, i.e. as if the two partners were alone in an infinite volume. This assumption is not exact, but it was extensively checked using JERK that this approximation remains quantitatively correct as long as the time interval Δt is not too large. Otherwise, the probability of encounter with a third partner would be no longer negligible.

The choice of Δt is a matter of compromise: too small a value would approach the limits of atomic Monte-Carlo or OKMC and too large a value would probe the delay probability law given above in a time window where it is less and less correct. In addition the number of events to be processed would grow too large. The actual values used for the simulations mentioned here are in the range 10^{-4}–10^{-2} s. An important difference between OKMC and EKMC is that the latter does not easily treat 1D motion, although in principle the corresponding probabilities can be calculated and introduced in parallel with the 3D ones.

The above procedure includes delay times of different types. Some delay times are associated with events defined by a frequency of occurrence consistent with a Poisson distribution (for example, the jump monitoring the emission of a monomer from a cluster), whereas the others account for encounters between objects which are the result of diffusion and not a Poisson process. It has been shown in the past that for problems where Poisson processes act in parallel, the RTA is equivalent to the brute force Metropolis scheme [26]. No formal proof has been established up to now for the case of event based Monte-Carlo. However, a recent reformulation of Jerk called First Passage Kinetic Monte-Carlo (FPKMC) has been numerically checked extensively against the RTA treatment of the same diffusion problem and no detectable difference could be found between the two approaches [27].

3. The code parameterization problem

The problem of determining an initial parameter set is common to any model used to simulate microstructure evolution. By parameter set we mean the whole set of physical mechanisms included in the model, along with the physical or materials parameters that quantitatively define them, such as characteristic energies, attempt frequencies and capture radii. Clearly, the appropriateness of a parameter set should be decided on the basis of its ability to reproduce available experimental results in a large enough range of conditions. However, as we shall discuss in this and the following sections, the work of identifying a suitable parameter set and of its corresponding validation is far from straightforward.

Several methods have been employed to simulate radiation damage by OKMC in pure Fe [28,29,9,30,10]. Experimentally, self-interstitial atom (SIA) loops have been long observed by transmission electron microscopy (TEM) to form under electron, neutron and ion irradiation in this material [31–34]. Precise experiments of *in situ* electron and ion irradiation of pure Fe thin foils at different temperatures (175–350 °C for electron irradiation and 200–400 °C for ion irradiation) have also been performed [35,36] and important information on the kinetics of SIA dislocation loop growth in this material as a function of temperature is available. Less quantitative information is available concerning vacancy clusters. Vacancy loops have been seen to form in Fe under heavy ion irradiation conditions at room temperature [37], but have not been observed under neutron irradiation [38], particularly in conditions relevant to reactor pressure vessel (RPV) steels in operation. Voids become clearly visible by TEM only at high doses, which are not attained in pressure vessel steels [39], although their presence in model alloys irradiated up to typical RPV steel doses, below

electron microscope resolution, is apparent in Positron Annihilation Spectroscopy (PAS) studies [40–43].

The experiment providing the most precise quantitative information from PAS on the vacancy cluster size distribution is one on pure Fe neutron-irradiated in the High Flux Irradiation Reactor (HFIR) in Oak Ridge National Laboratory, at relatively low temperature (<100 °C) [42,43]. It should be noted, however, that while this technique is valuable for observing very small vacancy clusters, it is unable to give a cluster size distribution above about ten vacancies, as the positron life-time changes are very small. We are in no-man's-land for sizes between those detectable by PAS and those detectable by TEM or Small Angle Neutron Spectroscopy (SANS). These latter methods can not identify vacancy cluster containing less than about 50 vacancies. Finally, a number of precise resistivity recovery studies have been performed in the past [44,45], which cast some light on the basic properties of single point-defects and which provide a relatively simple benchmark for microstructure evolution models. Thus, data on pure Fe for model validation are available. As discussed below, it is possible to obtain good agreement with the results of specific experiments, in terms of SIA loop or vacancy cluster density and size distribution, using sensible and physically-grounded parameter choices. However, the determination of a unique parameter set which is valid for any irradiation condition has so far proven elusive.

The problem becomes all the more difficult in the case of Fe alloys. The defects produced by irradiation in ferritic alloys, particularly steels, are difficult to characterize experimentally, even using the most advanced techniques currently available. They remain relatively small throughout the course of the irradiation, especially in the case of main interest here, i.e. that of neutron irradiation up to the doses of relevance for RPV steels (0.1–0.2 dpa). A complete characterization of radiation defects in Fe alloys as a function of dose requires the combined use of a large number of experimental techniques, since each technique is sensitive only to a certain class of defects, in a certain range of size. A key contribution of the Project was to provide the most complete collection of microstructural data on Fe-based alloys ever assembled. It includes a range of different techniques (TEM, PAS, tomographic atom probe, SANS, etc.), on alloys of increasing complexity (from pure Fe to steels), all neutron-irradiated at the same conditions, to a range of doses. The primary limitation is a single irradiation temperature (~300 °C) [46]. Under irradiation conditions typical of pressure vessels (though at a damage rate approximately two orders of magnitude higher), SIA loops are not observed in steels when they are observed in pure iron. Furthermore, it is well known and has been observed in many materials, particularly face-centered cubic materials, that the average size of visible SIA loops is reduced with increasing levels of impurities or alloying elements [47]. In addition, the Project's experimental program has provided detailed data on the mean size and number density of vacancy clusters including information about the associated solute atoms. The results suggest that a correct description of the association of solute atoms with point-defect clusters is of paramount importance to understand and explain the observed microstructure evolution in RPV steels [48]. This solute-atom/point-defect-cluster association, however, makes the parameterization of coarse-grained microstructure evolution models for irradiated materials even more delicate. Much data of fundamental importance to the simulations, such as the interaction strength of point-defects and point-defect clusters with solute atoms, cannot be obtained experimentally in a straightforward manner and their calculation requires a large number of possible cases to be considered. This is the case even for relatively simple alloys, such as Fe–Cu alloys, in spite of the growing number of experimental studies under irradiation in different conditions [41,49–53].

A complete account of the microstructural data available on irradiated Fe alloys for use in model validation and the corresponding attempts to model them is beyond the scope of this review. The main message we wish to convey is that despite the substantial collection of data available, the data are never sufficiently complete in terms of analyzed defects, dose and temperature ranges, and level of uncertainty associated with the measured values to fully evaluate the acceptability of the model predictions. In addition, many quantities, especially characteristic energies, cannot be measured experimentally and in many cases the actual mechanism responsible for a certain microstructure is uncertain. At the same time, blind fitting to experimental data cannot work with models of relatively high complexity, such as KMC models, where a large number of parameters are involved and the *a priori* selection of the physical mechanisms plays the most important role. Therefore, the only acceptable strategy is to introduce as much physical knowledge as possible from more fundamental studies into the models. This must be complemented by educated assumptions whenever the available data are insufficient to provide enough detail concerning characteristic energies and other material parameters. This approach leads to a kind of trial-and-error procedure, where it is not always possible to clearly identify the reason for either the success or the failure of the model. This inevitably involves other iterations of more fundamental studies in order to improve the physical understanding and the quantification of the physical mechanisms that correspond to the apparent weakness of the model. The need to perform this trial-and-error procedure is particularly stringent in the case of the effect of temperature, since many mechanisms involve Arrhenius-type exponential expressions and are thus very sensitive to this variable. This approach also exposes limitations inherent to the models, which may have remained hidden until a problem is encountered. For this purpose, *inter-model* comparisons prove extremely useful. Finally, with all the limitations that KMC models may have, they can in any case be valuable for parametric studies, particularly when geometrical correlations are expected to be of importance and therefore mean-field approximation models cannot provide an adequate answer. In the following sections, the difficulties in applying these models and the advances made in order to remove them within the Project are summarized. These include not only examples of comparisons between models and experimental data, but also an overview of the extensive work done to compare among models and to perform parametric studies. Before doing so, the different parameter sets adopted in the studies performed with the different codes are presented and briefly commented on. As a complete description of all the parameters for all the codes is beyond the scope of this article, we present only the most crucial parameters.

3.1. Parameter sets mainly adopted in LAKIMOCA

One of the main, and largely still enduring, question marks in the case of Fe alloys concerns the properties of SIA clusters, particularly their mobility. Different pictures existed for their behavior at the beginning of the project, largely based on MD studies with interatomic potentials and on the emerging evidence from *ab initio* calculations. In the case of LAKIMOCA, three first-attempt parameter sets were accordingly defined [11]. These tried to encompass the most common choices from OKMC and also MFRT models then available from the literature [28,29,9,35], as well as introducing first-approximation corrections taking into account *ab initio* evidence. In set I, following the results of Osetsky et al. [54], all SIA clusters (size $n \geqslant 2$) migrate in 1D, with a migration energy $E_m = 0.04$ eV and a prefactor decreasing with size according to the law: $\nu \cdot n^{-s}$ ($\nu_0 = 6 \times 10^{12}\,s^{-1}$, $s = 0.51$). Thus, set I embodies the picture of SIA cluster migration that was until recently widely

accepted based on MD results. In set II, small clusters ($n \leqslant 5$) migrate in 3D with $E_m = 0.4$ eV, as suggested by recent *ab initio* calculations [55], while larger clusters maintain 1D motion with $E_m = 0.04$ eV. For large clusters the prefactor decreases with $s = 0.51$ and for small ones ($\leqslant 5$) it decreases with $s = 10$. Finally, set III treats small clusters ($n \leqslant 5$) in the same way as set II, but assumes larger clusters to be completely immobile (see Table 1). For vacancy clusters, the same mobility has been used for all three sets: a migration energy of 0.65 eV and a prefactor decreasing with size according to the law $\nu_0 p^{-(n-2)}$ for $n \geqslant 2$, with $p = 100$ and $\nu_0 = \times 10^{12}\ s^{-1}$. The parameter values are summarized in Table 1. The various parameter choices can also be understood as accounting for materials containing different levels of impurities. Sets I and II correspond to extremely (and unrealistically) pure Fe, although the description of small clusters in set I is certainly incorrect for pure Fe, according to the latest *ab initio* data [56]. Set III corresponds to a level of impurities so high that loop mobility is effectively suppressed, which may be reasonable at low temperature, if their migration energy really is of the order of 1.3 eV, as suggested by recent experiments [57].

These three sets, with all their limitations, have been used for a large number of studies, providing sometimes reasonable agreement with experiments or allowing the effects of certain variables on long-term damage evolution to be identified. As will be seen, the choice of the set affects dramatically the results. The highlights of the work applying these parameter sets in LAKIMOCA for comparison with experiments or for the identification of the effect of certain variables are reviewed in Sections 4.1 and 6.1. The model inter-comparison work involving LAKIMOCA with mean field rate theory is reviewed in Sections 5.2.1 and 5.2.3.

3.2. Parameter sets mainly adopted in BIGMAC

The parameter set used in BIGMAC for radiation effects in α-Fe has been changing, as more information both from experiments and from simulations emerged. In the first calculations of α-Fe performed with this code [9], values for migration energies of both vacancies and self-interstitials were those obtained from MD with the available interatomic potentials [28]. Therefore, the migration of small self-interstitial clusters was mostly athermal. Although self-interstitial clusters of all sizes were considered mobile, it was assumed that when two of these clusters interact they form a junction and become immobile. This parameterization allowed for a comparison between the damage produced in Cu and in Fe under the same irradiation conditions. As observed experimentally the defect density in Fe was much lower than in Cu. The reason behind this good agreement is that the determining parameter in this case was the distribution of the damage after the collision cascade in these two materials. Cu forms vacancy clusters already visible under TEM from a single cascade, while in Fe both vacancy and self-interstitial clusters produced directly in-cascades are below the TEM resolution limit.

In the latest simulations, parameters obtained by *ab initio* calculations [58] have been included in the parameterization. Table 2 shows the values for the mobile vacancies and small self-interstitial clusters. Since the issue of the mobility of large self-interstitial clusters is still under debate, similarly to what was done with LAKIMOCA different parameterizations have been used for these clusters in order to study their effect. In particular, the amount of He desorbed from He-implanted Fe was studied based on different assumptions for SIA-cluster mobility [59]. Three different assumptions were used: (a) all SIA clusters were immobile (b) SIA clusters with more than three atoms were immobile, and (c) all SIA clusters were mobile, with values for sizes larger than 3 taken from MD calculations [60]. In all cases SIA clusters smaller than 3 move in 3D while larger ones move in 1D. These calculations showed that assumptions about SIA mobility dramatically affects the results, not only of the SIA component of the damage, but indirectly of other defects or impurities, in this case He. The parameterization presented in Table 2 was used to study ion implantation in α-Fe and to compare with experimental data [61]. In this case the mechanism of formation of ⟨100⟩ loops from the reaction between ⟨111⟩ loops proposed by Marian et al. based on MD simulations [62] was included in the model. The general conclusion of these studies, as reached in previous OKMC studies, including those performed with LAKIMOCA [11,60], is that it is only possible to reproduce the observed experimental data when some mechanism for immobilization or slowing down of large self-interstitial clusters is included in the model. Note that the size of those self-interstitial clusters considered immobile or with lower mobility differs for different authors.

The binding energies are also important parameters for the OKMC simulations. Binding energies for small clusters can be obtained by *ab initio* techniques [64,65,55,58]. For larger clusters, the data can be obtained from empirical interatomic potentials and then extrapolated [28,11]. However although different *ab initio* codes appear to give similar results, the difference in values obtained from empirical interatomic potentials can be more significant from one potential to another [66]. Examples of binding energies used during the Project are presented in Tables 4 and 5.

3.3. Parameter sets adopted in JERK

The choice of the parameters in JERK was made by trying to introduce sensible simplifications, in order to let them depend on

Table 1
Summary of parameter sets for the description of SIA clusters.

SIA cluster size	Set I			Set II			Set III		
(E_m in eV)	s	E_m	D	s	E_m	D	s	E_m	D
$n = 1$	–	0.3	3D	–	0.3	3D	–	0.3	3D
$2 \leqslant n \leqslant 5$	0.51	0.04	1D	10	0.4	3D	10	0.4	3D
$n > 5$	0.51	0.04	1D	0.51	0.04	1D	Immobile		

Table 2
Values of the migration energies used in the latest OKMC simulations with BIGMAC. Data from *ab initio* calculations [63].

SIA cluster size	E_m (eV)	D	Vacancy cluster size	E_m (eV)	D
1	0.34	3D	1	0.67	3D
2	0.42	3D	2	0.62	3D
3	0.43	3D	3	0.35	3D
			4	0.48	3D

Table 3
Migration energies for defects in Fe and carbon-doped Fe (eV).

E_m (n)	$n = 1$	$n = 2$	$n = 3$	$n = 4$	$n > 4$
I	0.34	0.42	0.43	Immobile	Immobile
V	0.67	0.63	0.35	0.48	Immobile
C	0.87	Immobile	Immobile	Immobile	Immobile

Table 4
Binding energies (eV) of defect clusters ('capil. approx.' stands for capillary approximation). The last column gives the formation energy for the defect and the dissolution energy for the carbon.

	$n = 2$	$n = 3$	$n = 4$	$n = 5$	E_f
E_b (I_n)	0.8	Capil. approx.	Capil. approx.	Capil. approx.	3.77
E_b (V_n)	0.3	0.67	1.29	2.02	2.07
E_b (C_n)	0.09	Capil. approx.	Capil. approx.	Capil. approx.	0.41

Table 5
Increase of binding energies for defect-carbon clusters (eV).

$I + C$	$I_2 + C$	$I_3 + C$	$I_4 + C$
E_b (n)			
0.20	0.33	Capil. approx	Capil. approx.
$V + C$	$VC + C$	$VC + V$	$VC_2 + V$
E_b (n)			
0.41	0.77	0.52	0.43

a minimum number of numerical values which can be calculated through *ab initio* approaches [63,67]. The binding and migration energies of small defect clusters are listed in Tables 3–5 for the case of Fe and carbon-doped Fe. A positive binding energy implies an attractive interaction. The capillary approximation[1] was used for larger clusters V_n and I_n whenever possible, but all the simulations did show that their role is apparently unimportant, at least under the conditions explored with JERK. As stated above, only 3D migration of the mobile objects was taken into account.

4. Application for the simulation of "model" experiments

4.1. Positron annihilation study of neutron-irradiated high-purity Fe specimens

As mentioned in Section 3, one particularly clean and complete experiment, very suitable for modeling, is the positron annihilation study performed by Eldrup and coworkers [42,43] on high-purity Fe specimens, neutron-irradiated in the range of about 0.0001–0.8 dpa in the HFIR at Oak Ridge National Laboratory. This work provides a precise and detailed experimental assessment of the density and size distribution of vacancy clusters (nanovoids) versus dose in Fe, which is extremely valuable for the validation of microstructure evolution models. For similarly irradiated pure Fe, the total density of visible clusters (mostly self-interstitial clusters) versus dose is also available [39].

A dose-rate corresponding to HFIR ($\sim 10^{-6}$ dpa/s) was used for OKMC simulations with LAKIMOCA, where 0.23 dpa were accumulated at 70 °C in a $\sim 1.22 \times 10^{-22}$ m^3 pure Fe box, with periodic boundary conditions. This equals the maximum dose for which results of void size distribution are provided in [42]. The HFIR spectrum was decomposed into 3×10^{16} FP cm^{-3} s^{-1}, 4×10^{14} 10 keV cascade-debris cm^{-3} s^{-1} and 2×10^{14} 20 keV cascade-debris cm^{-3} s^{-1}, in accordance with INCAS package results [68]. The simulation was first performed using sets I, II and III as described in Section 3.1. For set I and II, when no traps are introduced, no damage accumulation takes place. Even when including traps in set I and in set III, the saturation density versus dose is not reproduced. Only for set II, if traps for SIA and their clusters are introduced (in a concentration of 100 ppm and with a binding energy between trap and object of 0.9 eV, and a capture radius for traps of 5 Å), is a good agreement obtained with the experimental data, i.e. the saturation of the damage versus dose. This is shown in Fig. 2 for a number of slightly different choices of parameters that hardly affect the overall result.

The main outcome of these simulations is that it is necessary to allow for SIA cluster 1D (fast) migration, while introducing traps for them, in order to reproduce the reference experimental results. The capture radius is found to have a very limited effect on the results, although at low dose the smallest radius provides the best agreement, fully contained in the experimental error bar (Fig. 2). The vacancy cluster size distribution versus dose obtained from the simulation with set II and 100 ppm of SIA traps and the smallest capture radius is shown in Fig. 3. This figure can be directly compared with Fig. 4 in [42] and Fig. 6 in [43]. The agreement between simulation and experiment is excellent. The only noticeable difference between simulation results and experimental measurements is that the former tends to shift the size distribution towards somewhat larger clusters, thereby predicting a slightly lower density.

4.2. Isochronal recovery experiments

Isochronal recovery experiments correspond to relatively simple model experiments, in which damage is produced at low tem-

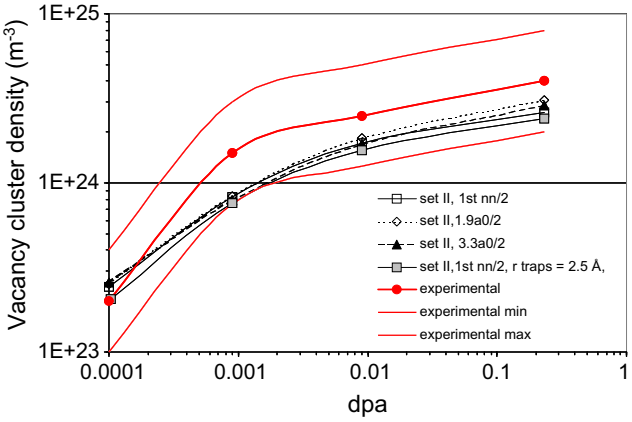

Fig. 2. Density of vacancy clusters in pure Fe at different doses after a neutron irradiation in HFIR at 70 °C including experimental uncertainty, as reported in Refs. [42,43]. OKMC with set II with traps for interstitials (binding energy of 0.9 eV and capture radius of 2.5 Å) for three different capture radii. Set II with traps for interstitials with a binding energy of 0.9 eV and a recombination distance of 2.5 Å is also represented in the figure. ($200a_0 \times 200a_0 \times 200a_0$ simulation box, periodic boundary conditions).

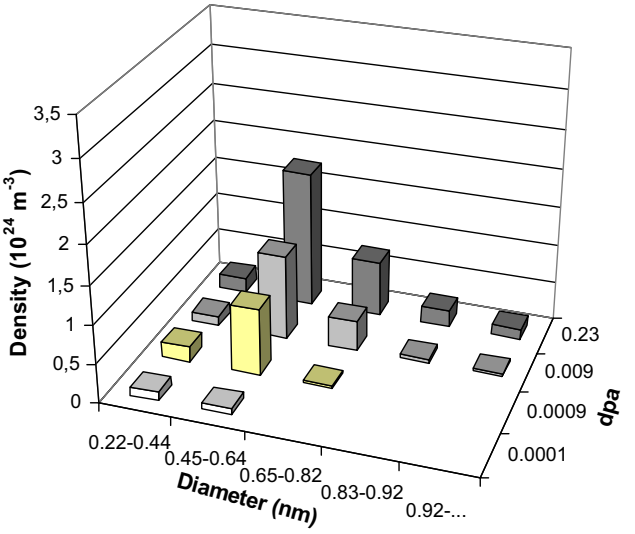

Fig. 3. Vacancy cluster size distribution versus dose according to the OKMC simulation using set II with traps and a 1nn capture radius. The size for a cluster of N vacancies is given by an equivalent diameter, i.e. the diameter of a sphere with a volume equal to N vacancies. To be compared with experimental results in Refs. [42,43].

[1] The capillary law is an empirical model assuming that the defect cluster containing n atoms is a spherical object, whose formation energy is proportional to the surface of the cluster. With this approximation, the binding energy $E_b(n)$ corresponding to adding an atom to a cluster of size $n-1$ is given by

$$E_b(n \to (n-1)+) = E_f(n-1) + E_f(1) - E_f(n)$$
$$= [(E_b(2) - E(1))((n)^{2/3} - (n-1)^{2/3})]/(2^{2/3} - 1) + E_f$$

when n becomes large the asymptotic limit will be $E_f(n = 1)$

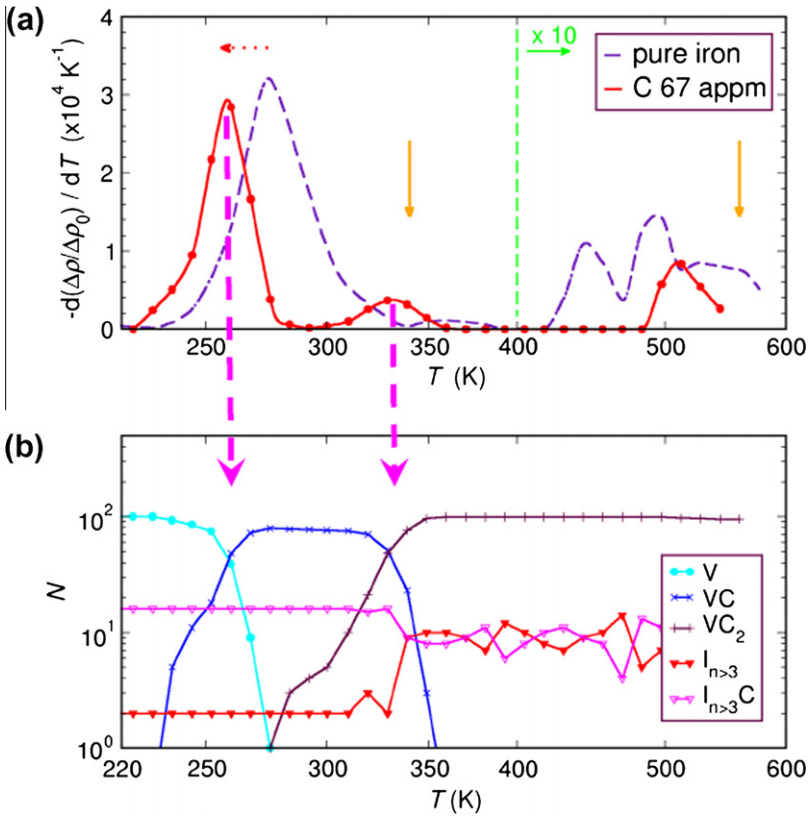

Fig. 4. (a) Simulated resistivity recovery stages in e-irradiated Fe and Fe–C alloys, where the dashed horizontal arrow indicates the shift of the stage III due to the presence of C, and the solid vertical arrows show experimental positions of the C migration stage and the cluster break up stage at 340 K and 560 K respectively. (b) The associated defect population evolution as predicted by the EKMC code JERK.

perature and then annealed. They are therefore amenable to modeling and are especially useful to verify the assumptions made in a model concerning point-defects and their small clusters, defects that can now be directly studied using *ab initio* methods [55,63,67]. Isochronal resistivity recovery experiments in pure Fe after electron irradiation were used for the validation of the EKMC code JERK and of the assumptions made in it, as described in Section 3.3. The effort was focused on electron irradiation because in this case the nature of defect creation (namely, isolated FPs at an experimentally determined separation distance) is not disputable. In experiments involving neutron or ion irradiation, on the other hand, the issues of cluster formation inside the cascades and of the extent of the dynamical recovery before any thermally controlled migration arises must be considered along with the question of the dimensionality of migrating clusters. Virtual samples with or without carbon were 'pre-irradiated' at 4 K (from 2×10^{-6} dpa to 200×10^{-6} dpa) and progressively annealed during increasing temperature steps up to 500 K, while the overall resistivity of the sample was recorded. At the end of the computer experiment, the derivative of the resistivity change with respect to temperature is plotted as a function of the absolute temperature: peaks are observed (named 'stages' hereafter), which correspond to a noticeable decrease of resistivity. The analysis consists of matching each stage with a well identified reaction or migration process. The simulation follows closely the experimental procedure, as shown in Fig. 4.

The initial condition of the simulation starts after stage I_E where only 60% of the injected defects are still present; the very first stages of the annealing (I_A–I_D) correspond to close pair recombination along dense rows of the lattice, a feature which is not reproduced in JERK, where no lattice is present. A fair quantitative agreement was found between simulation and experiment, in the case of pure Fe, even without invoking a 1D migration for large SIA clusters [63] because no formation of large SIA clusters takes place under these conditions. The same modeling approach was therefore used to address the problem of the effect of carbon atoms on vacancy mobility and clustering. V_nC_m clusters exhibit an attractive interaction for n and $m \leqslant 3$ [67], their binding energies are indeed larger than those between carbon and self-interstitials (Table 5). These V_nC_m clusters were considered as immobile and their role consisted only of trapping point-defects and releasing them at higher temperatures. Finally C_n clusters were found to be slightly attractive, in agreement with common sense (precipitation of ε-carbide at room temperature). The C_n clusters were also considered as immobile and their main role consisted of releasing individual mobile C atoms at higher temperatures.

All the experimental findings concerning the effects of C on the position of the recovery stages were qualitatively reproduced [44,63]. In particular, the stages related to the migration of vacancy and carbon and their interaction are shown in Fig. 4, namely:

(i) a shift of the stage III peak towards lower temperatures, this peak corresponds to a drop in resistivity which is not associated with the elimination of vacancies, but to their trapping at C atoms, the resistivity of the complex VC being definitely smaller than that of V and C far from each other;
(ii) an additional peak around 340 K depending on carbon concentration and probably linked to the formation of C_n clusters; and
(iii) the increase of the peak around 560 K attributed to the decomposition of V_nC_m complexes formed at lower temperatures.

It is worth mentioning that an important technical obstacle remain to be overcome. For the high *C* contents (67 ppm) at higher temperatures, the number of mobile species (mainly *C*) increases and a large fraction of the computer time is entirely devoted to treating the rapidly repeating events of *C* emission from C_n clusters and the reverse absorption reaction. This is the reason smaller computation cells were used, yielding poorer statistics. It is worth noting that the same difficulty was faced by the OKMC (BIGMAC code), which also could not extend the computations to larger cells and high temperatures.

5. Inter-model comparisons: KMC versus MFRT

As mentioned in Section 3, inter-model comparison is an extremely useful exercise to reveal the limitations of each model and, even more importantly, to suggest ways to complement one model with another in order to overcome the limitations of both. A few examples of these studies are reviewed in what follows.

5.1. Sink strength studies

Much of the developmental work concerning MFRT models has historically been on the sink strengths [12]. The sink strengths, defined as the square of the reciprocal of the mean distance covered by a defect before being absorbed by the considered sink, are key parameters for rate equations. They embody geometrical information included in an otherwise mean-field approximation, where changes of species concentrations are governed by rates of appearance and disappearance that are independent of the spatial distribution of the species. One of the advantages of OKMC models is supposed to be their capability of directly accounting for geometrical information. However, this needs to be verified. In particular, the SS for three-dimensionally (3D) and one-dimensionally (1D), or mixed 1D/3D, migrating defects in irradiated materials have attracted much attention in the recent past, because many experimental observations cannot be interpreted unless 1D or mixed 1D/3D migration patterns are assumed for self-interstitial atom clusters produced in-cascades during irradiation. Analytical expressions for the sink strengths for defects migrating in 3D and also in 1D have been therefore developed and a "master curve" approach has been proposed to describe the transition from purely 1D to purely 3D defect migration [69]. OKMC methods [70–72] have subsequently been used to corroborate the theoretical expressions but, although good agreement was generally found, the ability of this technique to reach the 1D migration limit has been questioned. The limited size of the simulation box used in OKMC studies has been blamed for the inadequacies of the model. The capability of OKMC to reproduce the sink strengths of spherical absorbers was therefore explored again using LAKIMOCA [15]. Conditions included a wide rage of volume fractions, together with the sink strength of grain boundaries, and with defects characterized by migration dimensionality from fully 3D to pure 1D. This work showed that the OKMC technique is not only capable of reproducing the theoretical expressions for the sink strengths in the whole range of conditions explored (Fig. 5), but is also sensitive enough to reveal the necessity of correcting the theoretical expressions for large sink volume fractions. This demonstrated that, in spite of the limited size of the OKMC simulation box, the method is suitable for describing the microstructure evolution of irradiated materials for any defect migration pattern. This includes accounting for the effect of extended microstructural features, which are much larger than the simulation box, such as grain boundaries, provided that some simple precautions are taken and that appropriate algorithms are introduced.

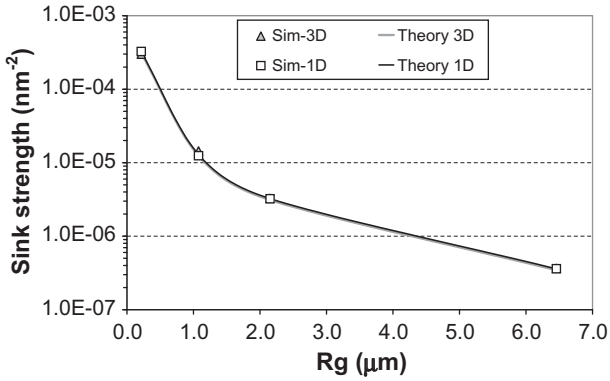

Fig. 5. Sink strength of a spherical grain boundary as a function of its radius for both 3D and 1D migrating defects. Lines corresponds to theoretical expressions, dots correspond to simulation results.

5.2. Microstructure evolution studies

Models employing the MFRT have been extensively used to describe radiation-induced phenomena such as void swelling and irradiation creep [73,74]. Although MFRT and KMC models can be used to simulate the same phenomena, many of the details are handled quite differently in the two approaches. For instance, in MFRT models, the point-defects and point-defect clusters made of *n* SIAs (I_n) or vacancies are characterized by their number density C_{ni} and C_{nv}. The changes of C_{ni} and C_{nv} with time are described by a set of ordinary differential equations. The physics is contained in the rate coefficients. The primary approximations in such models are the time and spatial averaging of the radiation damage source term, and the spatial averaging of the microstructure into an effective medium. KMC models can account for these spatial and temporal correlations very easily (see also previous section); their primary limitation is the computational burden, which is related to the size of the simulation volume. Even with modern computers, the maximum simulation volume size and the maximum dose (typically much less than 1 dpa) that can be simulated are limited. For example, an OKMC simulation cell size of $300 \times 300 \times 300$ lattice parameters, a_0, with $a_0 = 0.2876$ nm for α-Fe, leads to a simulation volume of 6.42×10^{-22} m^3. The minimum possible defect density that can be thus measured in OKMC simulations with this cell size is 1.56×10^{21} m^{-3} (one defect per simulation cell). In contrast, essentially any defect density can be simulated in the effective medium employed in the MFRT and even very detailed MFRT models can simulate microstructural evolution for doses up 100 dpa, or greater, in clock times that are relatively short.

5.2.1. Point-defect cluster dynamics modeling

A direct comparison of MFRT and OKMC (LAKIMOCA) simulations has been made in the domain of point defect cluster dynamics modeling, which is relevant to the evolution (both nucleation and growth) of radiation-induced defect structures [4]. The comparison of the two methods was restricted to the specific case of the evolution of the vacancy and SIA cluster size distribution functions in a pure metal under irradiation with a constant network dislocation density as the only fixed sink. The models were evaluated for the following conditions: (1) primary damage produced either (a) in the form of FP only; or (b) FP plus small clusters of either vacancies or SIAs typical of those generated by displacement cascades [75]; (2) the point-defects diffuse by three-dimensional (3-D) random walk; (3) the vacancy and SIA clusters are immobile; (4) the nucleation of vacancy and SIA clusters proceeds via a homogeneous mechanism in the case of 1(a), or by both homogeneous and in-cascade clustering mechanisms at the same time for 1(b); (5) vacancy clusters are treated as spherical neutral sinks for

point-defects; thermal emission of vacancies is determined by a size-dependent binding energy; (6) SIA clusters are treated as 3-D spherical clusters, with a preference (bias) for absorbing SIAs relative to vacancies, and are stable against thermal SIA emission; and (7) edge dislocations are a fixed matrix sink with a preference (bias) for SIAs that is the same as the SIA clusters.

The results shown in Fig. 6 illustrate the similarities and the differences between the OKMC and MFRT results at different irradiation temperatures and a relatively high damage rate of 4×10^{-5} dpa/s with only FP generation. The vacancy concentration is shown in Fig. 6a and the void number density in 6b. The sink structure used to obtain the results in Fig. 6 included vacancy and interstitial clusters, but no fixed dislocation sink. The MFRT and OKMC results are in reasonable agreement, with the vacancy concentration slightly higher for the OKMC model because of the difference in the vacancy cluster sink strength obtained in the two models, as discussed in Ref. [4]. The more realistic discrete lattice description of diffusion and sink geometry leads to a reduced effective sink strength for small point-defect clusters in the OKMC compared to that obtained from the mean field sink strength for small spherical sinks. For temperatures greater than about 200 °C, the predictions of the OKMC model show considerable scatter, due to the limited number of vacancies and vacancy clusters in the simulation cell. In fact, these results provide a useful measure of the number of objects required for the OKMC model to provide an adequate representation of the MFRT results. For example, in Fig. 6a, there is considerable scatter in the value of the vacancy concentration obtained from the OKMC model at 523 K. At this temperature, the number of vacancies in the simulation cell is about 100. At the higher temperature of 573 K, where there are about 50 vacancies in the simulation cell, the scatter in the vacancy concentration is ±50%. The vacancy cluster number density falls below one per OKMC cell volume for temperatures greater than 523 K.

An example of simulations involving cascade damage conditions is shown in Fig. 7. The conditions chosen for this comparison were an NRT displacement rate of 10^{-5} dpa/s, cascade efficiency of 0.4, and a temperature of 573 K. The spatial correlation of defects produced in-cascades was eliminated in the OKMC simulations. Although these special "randomized" cascades are less representative of real atomic displacement cascades, they provide a better simulation of how primary damage production is modeled in the MFRT. The agreement between the two models is somewhat improved, compared to the case when spatially correlated cascade damage was employed [4].

In-cascade production of point-defect clusters increases the cluster density, but, as shown in Fig. 6a, a temperature of 573 K leads to low point defect concentrations. The agreement between the OKMC and MFRT is relatively poor for the vacancy concentration and the self-interstitial density is too low to be accurately modeled using OKMC [4]. Values for the total cluster densities were in relatively good agreement because a sufficiently large number of clusters are formed, particularly voids. The number of vacancies and self-interstitials accumulated in clusters is in fair agreement as seen in Fig. 7a. However, a significant discrepancy is observed between the MFRT and OKMC results. The number of self-interstitials accumulated in SIA clusters should approach the number of vacancies in voids at high dose, with a slight excess in vacancy accumulation due to the dislocation-interstitial bias. This is the case for the MFRT curves in Fig. 7a, but the vacancy and self-interstitial curves are diverging for the OKMC model. Moreover, excess self-interstitial accumulation is observed for the OKMC case. This difference between the two models appears to arise from differences in the cluster size distributions shown in Fig. 7b [4]. The MFRT and OKMC results are in reasonable agreement only for small sizes, where a large number of clusters exist. However, the OKMC model cannot produce the smooth distribution seen in the MFRT predictions at larger sizes, because the density of large clusters is too low. Although the total number of clusters of both types exceeds the one-per-box volume criterion, the number at any given size is much lower. Spurious formation of large SIA and vacancy clusters arises from fluctuations in the OKMC results, and this leads to the higher level of accumulation predicted by the OKMC model. The discrepancy is greater for the SIA clusters because the MFRT model indicates that the cluster density should be essentially zero for SIA clusters larger than about 75.

This study verified the ability of alternate kinetic models based on the reaction rate theory and kinetic Monte-Carlo methods to obtain comparable results in well-posed simulations that are directly relevant to modeling radiation-induced microstructural evolution. Overall, the agreement between the two methods is best for irradiation conditions that produce a high density of defects (lower temperature and higher displacement rate) and for materials that have a relatively high density of fixed sinks such as dislocations. It has also helped to define irradiation regimes in which it may be inappropriate to use the OKMC methods. In particular, current computational limitations on the OKMC simulation cell size imply that it may be difficult to use the OKMC to simulate some aspects of microstructural evolution at the modest displacement rates and

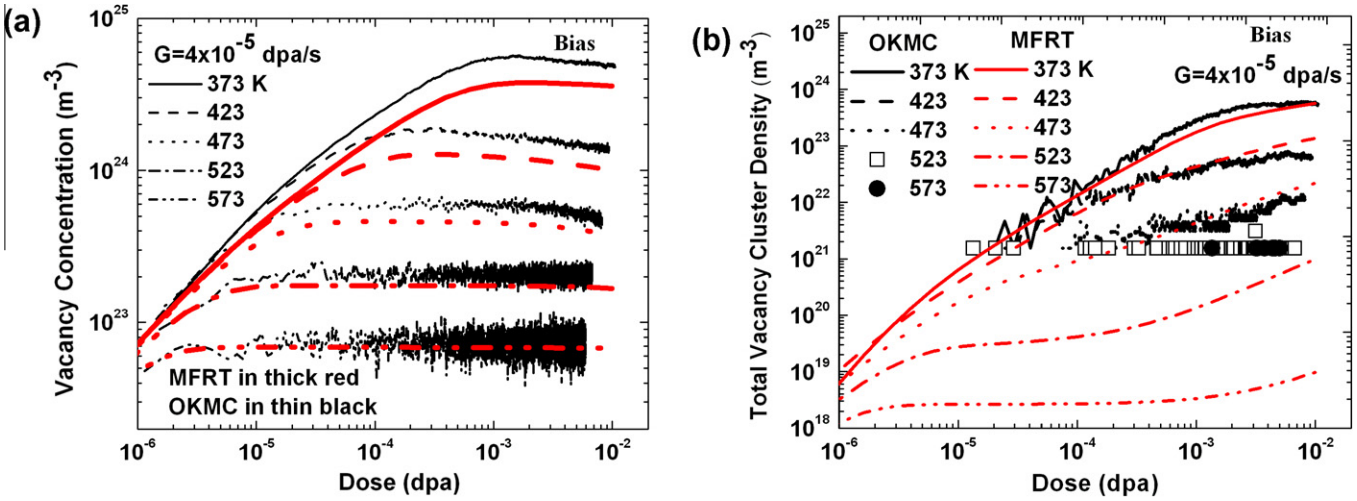

Fig. 6. Influence of irradiation temperature on MFRT and OKMC predictions of (a) vacancy concentration and (b) vacancy cluster density.

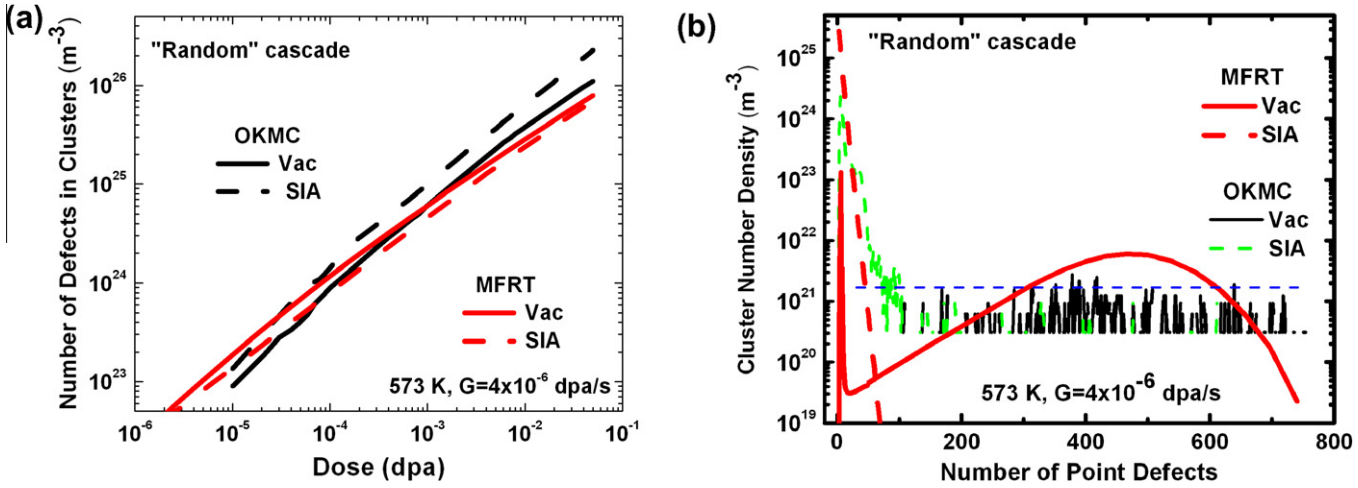

Fig. 7. MFRT and OKMC predictions of (a) point-defects accumulated in clusters and (b) cluster size distributions. Cascade damage production in which defects have no spatial correlation. Horizontal dashed blue line in (b) indicates one defect in OKMC box.

elevated temperatures relevant to many reactor components. For larger fluences and representative volumes, MFRT still appears indispensable. Expected advances in computing will expand the range of use for OKMC models, but this progress may occur slowly because orders of magnitude in defect density are required. However, the OKMC does a better job of accounting for spatial correlations (see also previous section), which can influence point defect reaction rates with small defect clusters and modify the primary damage source term under cascade damage conditions. As such, one immediate application of OKMC simulations is to improve the parameterization of the MFRT models.

5.2.2. Recovery of defects in ion-irradiated Fe

The recovery of damage produced by collision cascades in Fe has also been studied using both OKMC (BIGMAC) and MFRT approaches [19]. The initial damage distribution was obtained from molecular-dynamics simulations of 30 keV recoils in Fe. An isochronal annealing was simulated to identify the different thermally activated mechanisms that govern defect evolution. As in the recovery experiment on electron-irradiated Fe (see Section 4.2), the temperature was raised from 77 up to 800 K with isochronal steps of $\Delta t = 300$ s and temperature intervals such that $\Delta T/T = 0.03$. The defects produced by the 30 keV Fe irradiation were calculated by means of MD simulations. As a result, the final number of FP produced by the 30 keV Fe cascade after recombination and clustering was found to be 22. To simulate the evolution of these defects with the OKMC model, the position and size of each defect obtained by MD simulations were retained and used as initial conditions. Since in the MFRT approach only the mean concentration of defects can be followed, MFRT calculations were performed using as initial conditions the detailed concentration of SIAs, vacancy, SIA clusters (I_n) and vacancy clusters produced in the cascade. It is important to note that this averaging made in MFRT implicitly wipes out the existing spatial correlations between defects and implies that defects are homogeneously distributed. The parameters related to point defect motion are the ones presented in Table 2, except that only SIAs, di-SIAs and monovacancies were mobile.

The derivative of the total number of defects with temperature obtained by both methods is shown in Fig. 8 for an irradiation dose of 10^{-4} dpa. These curves indicate the different recombination mechanisms that take place during annealing. As expected, the MFRT model does not predict stage I_{D2} resulting from correlated recombination of interstitials and vacancies around $T = 115$ K.

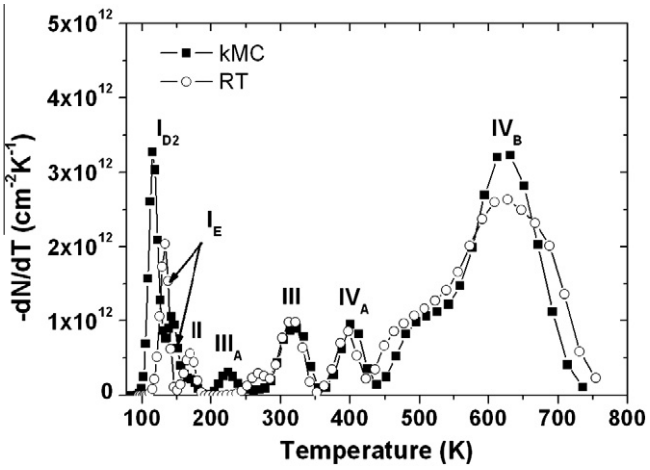

Fig. 8. Recovery stages predicted by OKMC and MFRT models for a 30 keV Fe irradiation for a dose of 10^{-4} dpa.

Stages I_E and II related to the migration of interstitials and di-interstitials, respectively, are however well predicted by the MFRT model, although their position is slightly shifted toward higher temperature. This is a dose effect. Stages III_A, IV_A and IV_B, not observed in the case of electron irradiation, are due to the initial clustering of defects in the cascade. As shown in Fig. 8, the position and the amplitude of peaks IV_A and IV_B predicted by the MFRT model are in very good agreement with the OKMC results. However, stage III_A predicted by OKMC at $T = 231$ K occurs in the MFRT model at a temperature of 264 K. Detailed OKMC simulations (not shown) reveal that this peak appears when the vacancy population drops. Since all SIAs and di-SIAs have already recombined at this temperature, this implies that vacancies recombine with immobile interstitial clusters $I_{n\geqslant 3}$. The fact that this peak is predicted at a higher temperature by the MFRT model—$T = 264$ K—strongly suggests that the peak predicted by the OKMC model results from the recombination of closely correlated vacancy-$I_{n\geqslant 3}$ arrangements that form during the collision cascade. To confirm this hypothesis, OKMC simulations were performed with initial conditions in which the defects created during irradiation were homogeneously and randomly distributed in space, i.e., without spatial correlations. Results are shown in Fig. 9 and compared to MFRT simulations. In that case, OKMC and MFRT results almost overlap. Both OKMC

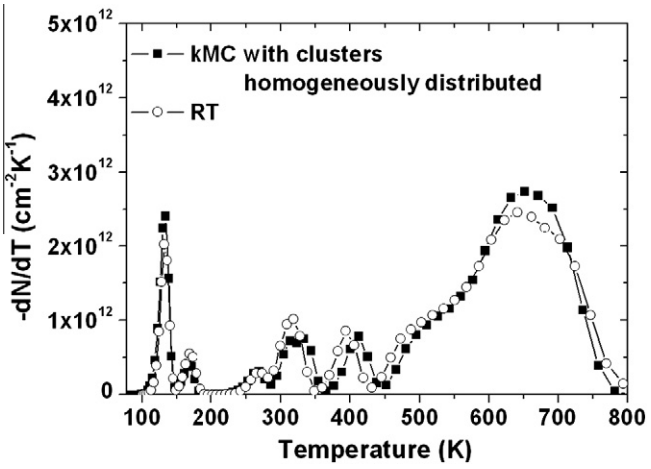

Fig. 9. Comparison between recovery curves for an irradiation dose of 10^{-4} dpa obtained with the OKMC model assuming all defects homogeneously distributed and the MFRT model.

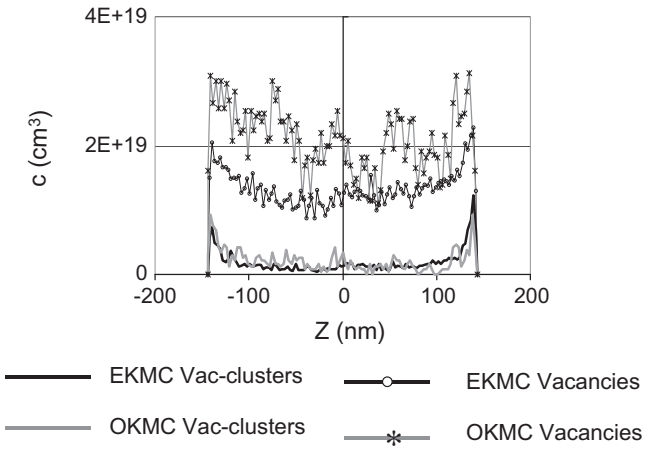

Fig. 10. Depleted and enriched zones in vacancies and vacancy clusters near the surfaces of the thin foil: vacancy and vacancy cluster concentration profiles across the thin foil at 200 °C after 120 s.

and MFRT models show a peak at $T = 264$ K with the same intensity and neither of them shows a peak at 231 K. Thus, peak III_A seen at $T = 231$ K in the OKMC calculations is due to the recombination of correlated vacancy-$I_{n\geqslant 3}$ arrangements that form in the cascade during irradiation, whereas the one observed at $T = 264$ K in the MFRT model is due to uncorrelated recombination between vacancies and $I_{n\geqslant 3}$. In the latter case, i.e., when defects are not correlated, the peak appears at a higher temperature since vacancies must migrate over a larger mean distance to find an interstitial cluster.

This comparison showed that the results obtained by the MFRT model are, overall, in good agreement with those obtained with the OKMC model, essentially because the comparison is made in conditions where sufficient statistics can be obtained in OKMC. Furthermore, this example clearly evidences the limitations of MFRT models, i.e., the lack of spatial correlations.

5.2.3. Comparison of MFRT, EKMC and OKMC

A comparison between MFRT and the two types of KMC procedures (JERK and LAKIMOCA) has been performed for a simple situation, a thin foil irradiated by electrons producing isolated FP [3]. The material considered was a model iron, free of dislocations. Impurities were not taken explicitly into account, except through the value of certain parameters. Only single point-defects were mobile and point-defect clusters were assumed to be spheres. The vacancy and the SIA of each FP were randomly put in the simulation cell. The input parameters describing the evolution of these objects are the same as those entering the MFRT formulation: reaction radii, diffusivities, and binding energies of clusters. The overall agreement between three very different modeling procedures is excellent for the slowest defect. The most important result is the spatial heterogeneity of vacancy clusters and the existence of a narrow temperature range where cavities are mostly nucleated close to the surfaces (Fig. 10). This last remark might be an alternative explanation for the big cavities observed in the vicinity of thin foil surfaces or grain boundaries at higher fluences.

There is still some disagreement between the two Monte-Carlo approaches for the density of interstitial clusters, which has to be understood before going further. The main difference between the three methods is the time which can be simulated as was already mentioned in Section 5.2.1. While the physical time which can be simulated is not limited for MFRT, the same is not true for EKMC and OKMC. For a given aimed-at delay time Δt, the two KMC codes behave differently: for OKMC, the CPU consumption is proportional to the number of jumps to be processed during Δt; while for EKMC, the CPU consumption is mostly an increasing function of the number of encounters. OKMC is expected to be more efficient at lower temperatures (or low mobilities, or high binding energies). Conversely, EKMC should be more efficient at higher temperatures with high mobilities.

This study also highlighted the necessity, for any future development, of obtaining a firm basis for determining the emission rates from defect clusters.

6. Parametric studies using OKMC models

Despite their overall simplicity and remaining flaws, the OKMC models described so far are useful for assessing the influence of specific parameters on the long-term evolution of primary damage, especially parameters that embody geometrical information and spatial correlations, which are therefore unsuitable to be handled using MFRT approaches. In what follows, a few examples of such studies are highlighted.

6.1. Influence of the internal displacement cascade structure on the growth of point-defect clusters in radiation environment

Radiation damage in materials starts with the interaction of neutrons with atoms, thereby producing displacement cascades. The so-called "primary damage" is the result of the displacement cascade (displacement cascade debris); it is produced within a timescale of a few picoseconds and is formed by a collection of vacancies and SIAs. The properties of these defects determine the growth of the clusters that they may form, and can be divided into two categories: geometrical properties (spatial distribution of defects in the cascade debris) and physical properties (diffusivities, capture radii, characteristic energies, etc.). An effort was made in the Project to understand the relative importance of the evolution of primary damage and long-term cluster growth, with the former not accounted for in a MFRT framework.

For a given primary knock-on atom (PKA), the cascade debris may be characterized by various quantities, such as the number of FP produced, their spatial extent or volume, their aspect ratio, their partitioning into sub-cascades, the fractions of clustered vacancies and SIAs and their pair distance correlations. Furthermore, it is well known that the primary knock-on atom (PKA) energy spectrum is broad, typically in the 5–100 keV range in RPV steels. Since the defects present in-cascade debris are transient objects, the above-mentioned quantities cannot be measured experi-

mentally, but they can be extracted from classical MD simulations with semi-empirical interaction potentials. The BCA can be also conveniently used to model the ballistic phase of the primary damage generation and can be implemented by an approximate model to describe the recombination occurring in the cooling phase [76,77]. Within the Project, groups of displacement cascades calculated independently with different interatomic potentials and different modeling strategies were compared on a statistical basis [78]. One group of cascades was generated in the BCA and all others by full MD. The MD results differed primarily due to the empirical interatomic potentials used and, to a lesser extent, to simulation strategies. At the end of the displacement cascades, the FP number distributions were systematically narrow. In contrast, the volumes, aspect ratios and fractions of clustered point-defects distributions were all positively skewed toward large values, with differences between modal and mean values on the order of 100% [76,79].

The following question thus arose: among the parameters characterizing the cascade debris, which ones have an influence on long-term microstructure evolution? In order to properly address this issue on a statistical basis, a large number of cascade debris must be studied. This is computationally cumbersome by MD, but can be done using the BCA within short computer times. A large set of BCA cascades were therefore used to explore the effects of cascade debris features on the long-term damage evolution. MD cascades were also used for comparison. Such a study was performed using the LAKIMOCA code [78,80–82]. The simulations were performed with the three different parameterizations of SIA and SIA-cluster mobility, as described in Section 3.1. The OKMC evolution was followed until 0.1 dpa were reached. It was found that using groups of cascades from different sources (MD and BCA) induced differences no larger than a factor of 2 in the cluster number densities. No clear correlation could be identified between the cascade debris characteristics (such as volumes, aspect ratios, or clustered point defect size distributions) and the number densities of vacancies and SIAs clusters predicted by OKMC at 0.1 dpa. However, the use of random point defect distributions instead of displacement cascade debris as input for the OKMC simulation led to significantly different results [78,80]. Hence, it was concluded that other aspects of the internal structure of cascades, not included in the addressed list, must correlate with the long-term evolution.

In order to further investigate this point, a large number of displacement cascades were generated in Fe by means of the MARLOWE BCA code with PKA energies ranging from 5 to 100 keV, to serve as input for the OKMC simulations [82]. One important result arising from this further study is that the size distributions of the vacancies and interstitials clustered in the long term are almost insensitive to the PKA energy in this range, as can be seen in Fig. 11, which was obtained with set II parameters. This was verified with the other OKMC parameters sets described in Section 3.1. Since the sub-cascade formation, morphology and spatial extension, as well as the spatial correlations between primary point defect positions, do depend on the PKA energy, it was concluded that the size distributions of point-defect clusters must not depend on these cascade parameters. It thus appears that the memory of the structure of displacement cascades progressively disappears over long times, in accordance with the principle of entropy maximization. This implies that simple cascade models could be used as input for the long-term evolution. The most extreme model is the mean-field approximation, where all spatial correlations between primary and evolving defects are ignored.

Remarkably, the cluster size distributions in the cascade debris were found to be independent of the PKA energy as well. OKMC simulations were then done, using either initial defect clusters with the spatial correlations induced by the cascades or redistributing the initial clusters at random in the OKMC simulation box. The results, shown in Fig. 12, provide evidence that the cluster spatial correlations do have significant consequences on the long-term evolution. The use of a mean-field approximation in cluster growth kinetics predictions, using source terms given by MD and/or BCA computation, is thereby invalidated, except in specific cases, such as the one addressed in Section 5.2.2. This effect could be at least partially overcome by using sources obtained after annealing of cascades or using some kind of effective source terms. These simulations showed that a limited amount of information regarding the PKA spectra and cascade debris characteristics needs to be known. In particular, neither the PKA momentum nor its energy are important. Consequently neither are the cascade debris characteristics which depend on the PKA energy such as the spatial extent, aspect ratio, splitting into sub-cascades, or pair distance correlations between point-defects. In contrast, the spatial correlations between the clusters of point-defects may have dramatic consequences on cluster growth in the long-term evolution. Which spatial correlations have the most influence on the long-term evolution is, however, a question which remains to be answered.

6.2. Effect of dose and dose rate

The influence of damage rate on the microstructure evolution of materials in general and RPV steels in particular is a long-standing issue. In the case of RPV steels, which are exposed to relatively low

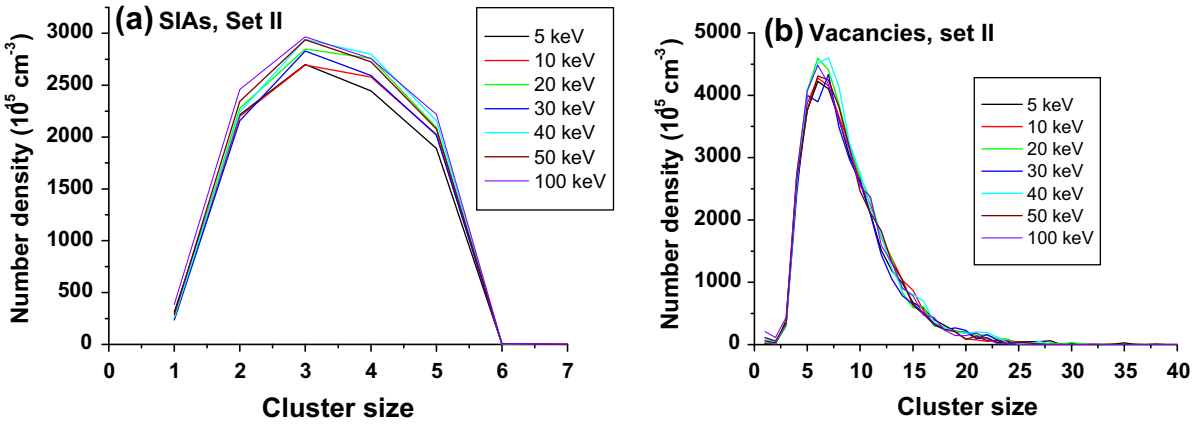

Fig. 11. Size distributions of SIAs and vacancies in clusters obtained by OKMC simulations using BCA cascades generated by PKAs with 5–100 keV energy. The dose rate was 10^{-6} dpa/s and the dose is 0.1 dpa. (a) SIAs and (b) vacancies. Similar results were obtained using MD cascades generated by PKA energies in the same range.

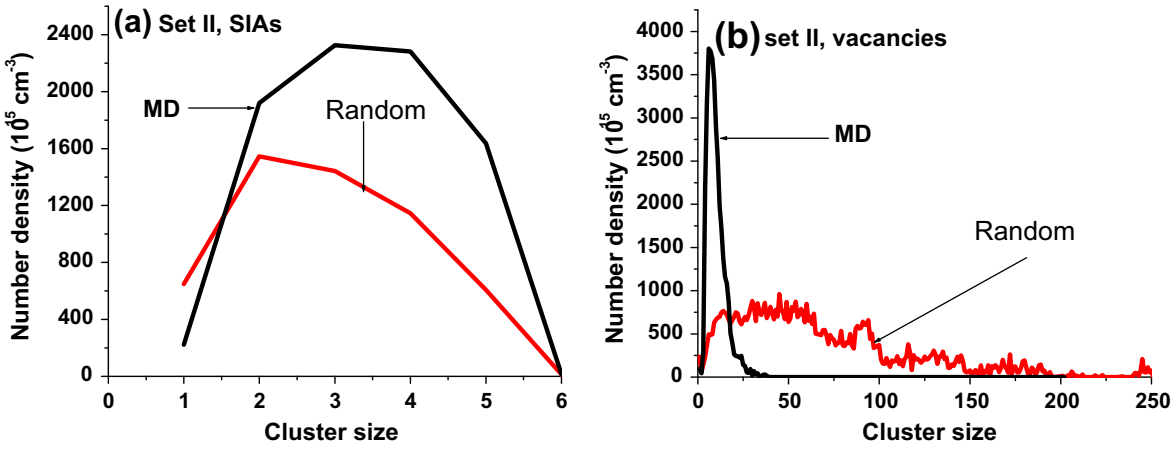

Fig. 12. Size distributions of SIAs and vacancies in clusters obtained by OKMC either by using 20 keV MD cascades as input or redistributing the point-defect clusters in the cascade debris at random in the whole OKMC simulation box. Dose and dose rate were, respectively, 0.1 dpa and 10^{-6} dpa/s. (a) SIAs and (b) vacancies. Similar results are obtained with the other OKMC parameters sets discussed in Section 3.1.

neutron fluxes, one potential issue is the applicability of test reactor data (where the damage rates are higher) to anticipate the behavior of steels under operating conditions. For neutron fluxes much greater than in RPV operating conditions (>100 times higher), a regime exists in which the effects of flux are well defined experimentally and are well predicted by current models. These same models predict that the effect of flux should be relatively weak for values near those obtained in commercial RPVs, but may increase at lower fluxes. However, it is difficult to obtain sufficient data at low to intermediate fluxes to unambiguously determine the effects of flux, since the time required to reach the desired fluences is necessarily long. KMC or MFRT models can be used to provide insight into this problem. LAKIMOCA was used to study the influence of dose rate on the prediction of neutron irradiation damage production in α-Fe. Damage rates ranging from 6×10^{-11} to 6×10^{-5} dpa/s were simulated. The three parameter sets presented above (Section 3.1) were used. Three dislocation segments were introduced in the simulation box. Our results indicate that the larger the damage rate, the more SIA clusters are formed (Fig. 13). The total number of SIAs, regardless of size, also increases with damage rate. For the vacancies, larger damage rates induce the formation of more clusters also (all sizes taken into account). However, clusters of size larger than approximately 10 vacancies are more numerous at low damage rates than at high damage rates. These results hold whatever the parameter set used, although with quantitative differences. The results of the analysis are consistent with a non-negligible effect of dose rate on microstructure, for fluxes near those typical of commercial RPVs. Up to what extent this affects embrittlement in RPV steels remains, however, difficult to tell, especially because in steels microstructural features involving solute atoms (precipitates), not included in this study, have the largest effect on embrittlement.

6.3. Equivalence between effective migrating energies and the use of traps

LAKIMOCA was also used to check the influence of traps for vacancies on a vacancy diffusing in an otherwise pure Fe matrix. One such trap with a binding energy of 0.6 eV in a box $20a_o \times 20a_o \times 20a_o$ wide was introduced in the simulation box. Its capture radius was 2.03 Å. A single vacancy was introduced, with a migration energy of 0.65 eV. Seven temperatures were studied ranging from 473 K to 773 K. For each temperature, the trajectory of the vacancy was recorded every Δt, and the mean square displacement (MSD) was calculated versus delay τ_k using the typical running average method. The diffusion coefficient is given by

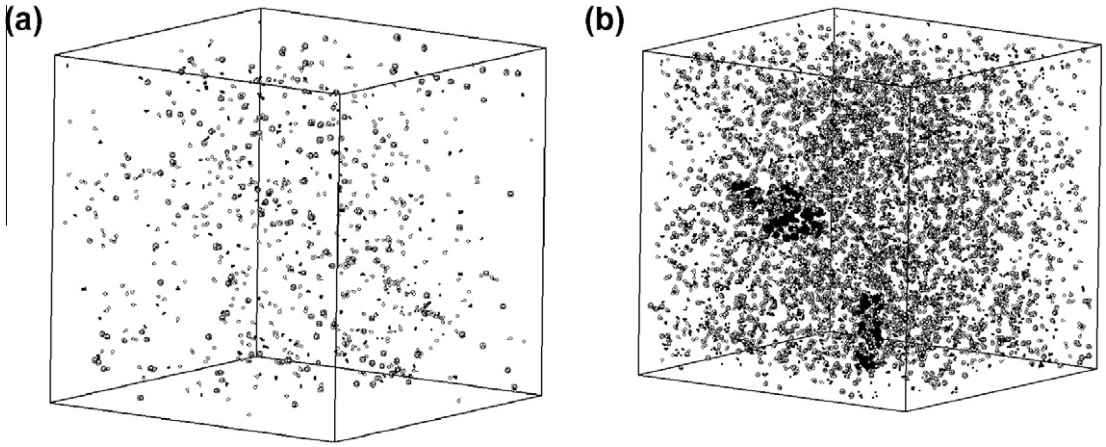

Fig. 13. (a) Microstructure after 0.1 dpa using set II and a damage rate of 6×10^{-11} dpa/s. The white spheres are vacancies, the black ones are interstitials and the slate grey small spheres are SIA traps. (b) Microstructure after 0.1 dpa using set II and a damage rate of 6×10^{-5} dpa/s. The white spheres are vacancies, the black ones are interstitials and the slate grey small spheres are SIA traps.

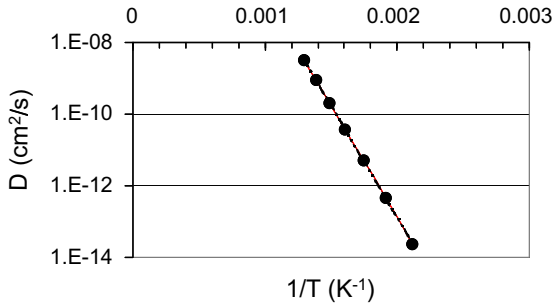

Fig. 14. Diffusion coefficient versus inverse temperature for temperatures ranging from 473 K to 773 K. The resulting effective migration energy for the vacancy is 1.25 eV.

the slope of the MSD and its evolution versus inverse temperature for the temperatures studied is shown in Fig. 14. The resulting effective migration energy for the vacancy was found to be, not surprisingly, 1.25 eV. This result validates the use of generic traps to model the effect of impurities in an OKMC model.

7. Discussion

Following this overview of what has been achieved during the Project, it appears that a number of issues still need to be addressed:

(i) Comparison of KMC with experiments. It is possible to find good agreement between simulations and experiments, in some especially clean and simple cases, particularly at low temperature. However, it has not been possible to determine a parameter set that can be used for all irradiation conditions, particularly if the temperature is increased. This may also be consequence of the limitation of KMC models. Concerning the physical mechanisms, the main remaining open question is the one related to SIA cluster mobilities and their mutual reactions. This is currently, as a palliative, addressed in OKMC with the introduction of traps or by making them immobile, both being clearly not satisfactory solutions. In addition, the parameter sets I to III used with LAKIMOCA, whose validity could not be clearly assessed, lead to predictions of defect densities that may differ by several orders of magnitude at higher doses.

(ii) Comparison of KMC with MFRT. It is worth noting that the good agreement reached between MFRT and OKMC when tracing the resistivity recovery stages in the presence of cascade damage must be regarded as very specific to this kind of experiment, where the damage is introduced at once at low temperature. This results in a large number density of immobile defects that are not far from being homogeneously distributed. Such agreement is not likely to be obtained under irradiation where cascades are introduced continuously. The comparison of these two approaches leads to a fairly obvious conclusion, which can now be better quantified. KMC is limited by large CPU time and simulation cell size, which may produce artifacts, particularly at high T and, in general, when the density of defects is too low to have sufficient statistics. MFRT does not account for correlated recombination or the spatial correlation of the initial cluster distribution in-cascades, which is seen to have an influence on long-term microstructure evolution. Both models are therefore needed, as they can complement each other and can possibly even be combined for better results. In particular, systematic KMC studies can be used to parameterize MFRT to mitigate its lack of spatial correlation. This does not prevent, and in fact encourages, the use of KMC for the simulation of experimentally relevant conditions and its comparison with experiments. Further work may overcome its limitations, e.g. by means of parallelization or by using other methodologies currently proposed in the literature, such as the FPKMC [27].

(iii) Primary damage simulation. As a result of computational advances, the state of the art in producing defect cascades by MD has improved over the last decades, accounting for the complete PKA energy spectrum. Notwithstanding this noticeable improvement (when compared to the initial binary collision codes), the present state of radiation damage simulation is probably still not sufficient. As an example, when using the output of simulated cascades [83] as input data for MFRT, the concentration of interstitial loops obtained was larger than the experimental ones by orders of magnitude [36]. The time window between the defect production and the dynamic annealing, and the start of the thermal annealing stage is not yet properly treated. During this time, the lattice is probably still perturbed by dynamical excitations which are not completely thermalized, such as sub-threshold collisions below 40 eV. Although these collisions do not form new defects, they may assist thermal diffusion processes and increase the apparent mobility of point-defects and of their clusters [84]. This time window must be treated by MD until the atom velocities in the cascade region are thermalized; the duration of this phase is controlled by thermal conductivity. Only from this point forward can the remaining cascade annealing be treated by KMC because it rests on the assumption of jump frequencies in a truly thermalized system.

8. Conclusions

Kinetic Monte-Carlo and mean field rate theory models are useful tools for simulating microstructure evolution of Fe alloys under irradiation. This review has shown that both of these two families of techniques are insufficient to fully model radiation damage. However, they are complementary and their combined use on well-defined cases may lead to the development of acceptable microstructure evolution models. A most important aspect of performing these simulations is the parameterization, including physical mechanisms and the characteristic parameters. Parameter values can be determined in simple cases and for small entities from *ab initio* calculations and experiments. Although substantial progress has been made during the Project, some important issues, such as the mobility and stability of SIA clusters, remain to be completely understood.

Acknowledgments

This work was performed in the framework of the Perfect IP, partially funded by the European Commission within the 6th Framework Program (contract nr. FI6O-CT-2003-508840). Support for Stoller and Golubov was provided by the Office of Fusion Sciences, US Department of Energy.

References

[1] Soisson et al., J. Nucl. Mater. 406 (2010) 55.
[2] Barbu et al., J. Nucl. Mater. 406 (2010) 39.
[3] A. Barbu, C.S. Becquart, J.L. Bocquet, J. DallaTorre, C. Domain, Philos. Mag. 85 (2005) 541.
[4] R.E. Stoller, S.I. Golubov, C. Domain, C.S. Becquart, J. Nucl. Mater. 382 (2008) 77.
[5] K.A. Fichthorn, W.H. Weinberg, J. Chem. Phys. 95 (2) (1991) 1090.
[6] F. Soisson, J. Nucl. Mater. 349 (3) (2006) 235.
[7] C. Domain, C.S. Becquart, J.-C. van Duysen, Mater. Res. Soc. Symp. Proc. 540 (1999) 643.

[8] C. Domain, C.S. Becquart, J.-C. van Duysen, Mater. Res. Soc. Symp. Proc. 650 (2001) R3.25.1.
[9] M.J. Caturla, N. Soneda, E. Alonso, B.D. Wirth, T. Díaz de la Rubia, J.M. Perlado, J. Nucl. Mater. 276 (2000) 13.
[10] N. Soneda, S. Ishino, A. Takahasi, K. Dohi, J. Nucl. Mater. 323 (2003) 169.
[11] C. Domain, C.S. Becquart, L. Malerba, J. Nucl. Mater. 335 (2004) 121.
[12] A.D. Brailsford, R. Bullough, Philos. Trans. Roy. Soc. Lond. 302 (1981) 87. and references therein.
[13] M.H. Kalos, P.A. Whitlock, Monte Carlo Methods, vol. I, Basics, John Wiley & sons, 1986.
[14] W.M. Young, E.W. Elcock, Proc. Phys. Soc. 89 (1966) 735.
[15] L. Malerba, C.S. Becquart, C. Domain, J. Nucl. Mater. 360 (2007) 159.
[16] M.D. Johnson, M.-J. Caturla, T. Diaz de la Rubia, J. Appl. Phys. 84 (1998) 1963.
[17] M.-J. Caturla, M.D. Johnson, T. Diaz de la Rubia, Appl. Phys. Lett. 72 (1998) 2736.
[18] M.-J. Caturla, M. Wall, E. Alonso, T. Diaz de la Rubia, T. Felter, M. Fluss, J. Nucl. Mater. 276 (2000) 186.
[19] C.J. Ortiz, M.-J. Caturla, Phys. Rev. B 75 (2007) 184101.
[20] E. Alonso, M.-J. Caturla, T. Diaz de la Rubia, J.M. Perlado, J. Nucl. Mater. 276 (2000) 221.
[21] C. Arévalo, M.J. Caturla, J.M. Perlado, J. Nucl. Mater. 351 (2007) 293.
[22] Cristina Arévalo, PhD Thesis, Universidad Politécnica de Madrid, 2007.
[23] J.F. Ziegler, J.P. Biersack, U. Littmark, in: J.F. Ziegler (Ed.), The Stopping, Range of Ions in Solids, vol. 1, Perfamon, New York, 1985, p. 22.
[24] J.M. Lanore, Rad. Effects 22 (1974) 153.
[25] J. Dalla Torre, J.-L. Bocquet, N.V. Doan, E. Adam, A. Barbu, Philos. Mag. 85 (2005) 549.
[26] M. Athenes, P. Bellon, G. Martin, Philos. Mag. A76 (1997) 565.
[27] T. Opplestrup, V. Bulatov, G.H. Gilmer, M.H. Kalos, B. Sadigh, Phys. Rev. Lett. 97 (2006) 230602.
[28] N. Soneda, T. Diaz de la Rubia, Philos. Mag. A 78 (1998) 995–1019.
[29] F. Gao, D.J. Bacon, A.V. Barashev, H.L. Heinisch, Mater. Res. Soc. Symp. Proc. 540 (1999) 703–708.
[30] J. Marian, B.D. Wirth, J.M. Perlado, T. Díaz de la Rubia, R. Schäublin, D. Lodi, M. Hernández, G. de Diego, D.G. Briceño, R.E. Stoller, Mater. Res. Soc. Symp. Proc. 650 (2001) R3.2.1–R3.2.6.
[31] B.L. Eyre, R. Bullough, Philos. Mag. 12 (1965) 31.
[32] I.M. Robertson, M.A. Kirk, W.E. King, Scr. Met. 18 (1984) 317.
[33] Y. Shimomura, H. Fukushima, M.W. Guinan, J. Nucl. Mater. 174 (1990) 210.
[34] L.L. Horton, J. Bentley, K. Farrell, J. Nucl. Mater. 108–109 (1982) 222.
[35] A. Hardouin Duparc, C. Moingeon, N. Smetniansky-de-Grande, A. Barbu, J. Nucl. Mater. 302 (2002) 143.
[36] E. Meslin, PhD 2007, Rouen University, 2007.
[37] M.L. Jenkins, C.A. English, B.L. Eyre, Philos. Mag. A 38 (1978) 97.
[38] A.C. Nicol, M.L. Jenkins, M.A. Kirk, Mater. Res. Soc. Symp. Proc. 650 (2001) R1.3.1–R1.3.6.
[39] M. Victoria, N. Baluc, C. Bailat, Y. Dai, M.I. Luppo, R. Schäublin, B.N. Singh, J. Nucl. Mater. 276 (2000) 114.
[40] A. Hempel, M. Saneyasu, Z. Tang, M. Hasegawa, G. Brauer, F. Plazaola, S. Yamaguchi, F. Kano, A. Kawai, Effects of radiation on materials, in: M.L. Hamilton, A.S. Rosinski, S.T. Rosinski, M.L. Grossbeck (Eds.), 19th International Symposium, ASTM STP 1366, ASTM, West Conshohocken, PA, 2000, p. 560.
[41] Y. Nagai, Z. Tang, M. Hasegawa, T. Kanai, M. Saneyasu, Phys. Rev. B 63 (2001) 134110.
[42] M. Eldrup, B.N. Singh, S.J. Zinkle, T.S. Byun, K. Farrell, J. Nucl. Mater. 307–311 (2002) 912.
[43] M. Eldrup, B.N. Singh, J. Nucl. Mater. 323 (2003) 346.
[44] S. Takaki, J. Fuss, H. Kugler, U. Dedek, H. Schultz, Rad. Effects 79 (1983) 87.
[45] H. Matsui, S. Takehana, M.W. Guinan, J. Nucl. Mater. 155–157 (1988) 1284.
[46] F. Bergner, A. Ulbricht, A. Gokhman, D. Erak, J. Nucl. Mater. 373 (2008) 199.
[47] E. Meslin et al., J. Nucl. Mater. 406 (2010) 73; M. Lambrecht et al., J. Nucl. Mater. 406 (2010) 84..
[48] M. Lambrecht, L. Malerba, A. Almazouzi, J. Nucl. Mater. 378 (2008) 282.
[49] F. Maury, N. Lorenzelli, M.H. Mathon, C.H. de Novion, P. Lagarde, J. Phys.: Condens. Mater. 6 (1994) 569.
[50] P. Auger, P. Pareige, S. Welzel, J.-C. Van Duysen, J. Nucl. Mater. 280 (2000) 331.
[51] N. Lê, A. Barbu, D. Liu, F. Maury, Scr. Metall. Mater. 26 (1992) 771.
[52] W.J. Phythian, A.J.E. Foreman, C.A. English, J.T. Buswell, M. Hetherington, K. Roberts, S. Pizzini, Effects of radiation on materials, in: R.E. Stoller, A.S. Kumar, D.S. Gelles (Eds.), 15th International Symposium, ASTM STP 1125, ASTM, Philadelphia, 1992, p. 131.
[53] K. Fukuya, K. Ohno, H. Nakata, S. Dumbill, J.M. Hyde, J. Nucl. Mater. 312 (2003) 163.
[54] Yu.N. Osetsky, D.J. Bacon, A. Serra, B.N. Singh, S.I. Golubov, J. Nucl. Mater. 276 (2000) 65.
[55] C.-C. Fu, F. Willaime, P. Ordejón, Phys. Rev. Lett. 92 (2004) 175503.
[56] D.A. Terentyev, T.P. Klaver, P. Olsson, M.-C. Marinica, F. Willaime, C. Domain, L. Malerba, Phys. Rev. Lett. 100 (2008) 145503.
[57] K. Arakawa, K. Ono, M. Isshiki, K. Mimura, M. Uchikoshi, H. Mori, Science 318 (2007) 956.
[58] C.C. Fu, F. Willaime, Phys. Rev. B72 (2005) 064117.
[59] M.J. Caturla, C.J. Ortiz, J. Nucl. Mater. 362 (2007) 141.
[60] N. Soneda, T. Díaz de la Rubia, Philos. Mag. A 81 (2001) 331.
[61] M. Hernández-Mayoral, M.J. Caturla, D. Gómez-Briceño, J.M. Perlado, E. Martínez, J. Marian, Proceedings of the Structural Materials for Innovative Nuclear Systems Workshop, OECD, Nuclear Energy Agency, pp. 275–282.
[62] J. Marian, B.D. Wirth, J.M. Perlado, Phys. Rev. Lett. 88 (2002) 255507.
[63] C.C. Fu, J. DallaTorre, F. Willaime, J.L. Bocquet, A. Barbu, Nat. Mater. 4 (2005) 68.
[64] C. Domain, C.S. Becquart, Phys. Rev. B 65 (2002) 024103.
[65] C. Domain, C.S. Becquart, J. Foct, Phys. Rev. B 69 (2004) 144112.
[66] L. Malerba et al., J. Nucl. Mater. 406 (2010) 7.
[67] C.C. Fu, E. Meslin, A. Barbu, F. Willaime, V. Oison, Solid State Phenom. 139 (2008) 157.
[68] S. Jumel, J.-C. van Duysen, J. Nucl. Mater. 238 (2004) 251.
[69] H. Trinkaus, B.N. Singh, A.J.E. Foreman, J. Nucl. Mater. 199 (1992) 1;
H. Trinkaus, B.N. Singh, A.J.E. Foreman, J. Nucl. Mater. 206 (1993) 200;
H. Trinkaus, B.N. Singh, A.J.E. Foreman, J. Nucl. Mater. 249 (1997) 91;
H. Trinkaus, B.N. Singh, A.J.E. Foreman, J. Nucl. Mater. 251 (1997) 172;
H. Trinkaus, H.L. Heinisch, A.V. Barashev, S.I. Golubov, B.N. Singh, Phys. Rev. B 66 (2002) 060105(R).
[70] H.L. Heinisch, B.N. Singh, S.I. Golubov, J. Nucl. Mater. 283–287 (2000) 737.
[71] H.L. Heinisch, B.N. Singh, J. Nucl. Mater. 307–311 (2002) 876.
[72] H.L. Heinisch, B.N. Singh, Philos. Mag. 83 (31–34) (2003) 3661.
[73] R.E. Stoller, G.R. Odette, A composite model of microstructural evolution in austenitic stainless steel under fast neutron irradiation, in: F.A. Garner, N.H. Packan, A.S. Kumar (Eds.), Radiation-Induced Changes in Microstructure, 13th International Symposium, ASTM STP 955, ASTM, Philadelphia, 1987, pp. 371–392.
[74] R.E. Stoller, M.L. Grossbeck, L.K. Mansur, A theoretical model of accelerated irradiation creep at low temperatures by transient interstitial absorption, in: R.E. Stoller, A.S. Kumar, D.S. Gelles (Eds.), Effects of Radiation on Materials, 15th International Symposium, ASTM STP 1125, ASTM, Philadelphia, 1992, pp. 517–529.
[75] R.E. Stoller, J. Nucl. Mater. 276 (2000) 22.
[76] A. Souidi, M. Hou, C.S. Becquart, C. Domain, J. Nucl. Mater. 295 (2001) 179.
[77] M. Hou, D. Kulikov, J. Nucl. Mater. 336 (2005) 125.
[78] A. Souidi, C.S. Becquart, C. Domain, D. Terentyev, L. Malerba, A.F. Calder, D.J. Bacon, R.E. Stoller, Yu.N. Osetsky, M. Hou, J. Nucl. Mater. 355 (2006) 89.
[79] C.S. Becquart, A. Souidi, M. Hou, Phys. Rev. B66 (2002) 134104.
[80] C.S. Becquart, C. Domain, L. Malerba, M. Hou, Nucl. Instr. Methods B228 (2005) 181.
[81] C.S. Becquart, A. Souidi, C. Domain, M. Hou, L. Malerba, R.E. Stoller, J. Nucl. Mater. 351 (2006) 39.
[82] M. Hou, A. Souidi, C.S. Becquart, C. Domain, L. Malerba, J. Nucl. Mater. 382 (2008) 103.
[83] C. Domain, J. Ruste, C.S. Becquart, Etude par simulation numérique du dommage d'irradiation: application au fer pur et aux alliages fer-cuivre, Technical Report, 1998.
[84] A. Tenenbaum, N.V. Doan, Philos. Mag. 35 (1977) 379.